Theoretical Study of the Mechanism of Exemestane Hydroxylation Catalyzed by Human Aromatase Enzyme

*Ignacio Viciano and Sergio Martí**

Departament de Química Física i Analítica, Universitat Jaume I, 12071 Castelló, Spain.

* to whom correspondence should be addressed

smarti@uji.es

Abstract

Human aromatase (CYP19A1) aromatizes the androgens to form estrogens via a three-step oxidative process. The estrogens are necessary in humans, mainly in women, because of the role they play in the sexual and reproductive development. However, these also are involved in the development and growth of hormone-dependent breast cancer. Therefore, inhibition of the enzyme aromatase, by means of drugs known as aromatase inhibitors, is the frontline therapy for these types of cancers. Exemestane is a suicidal third-generation inhibitor of aromatase, currently used in the breast cancer treatment. In this study, the hydroxylation of exemestane catalyzed by aromatase has been studied by means of hybrid QM/MM methods. The Free Energy Perturbation calculations provided a free energy of activation for the hydrogen abstraction step (rate-limiting step) of 17 kcal/mol. The results reveal that the hydroxylation of exemestane is not the inhibition stage suggesting a possible competitive mechanism between the inhibitor and the natural substrate androstenedione in the first catalytic subcycle of the enzyme. Furthermore, the analysis of the interaction energy for the substrate and the cofactor in the active site, shows that the role of the enzymatic environment during this reaction consists of a transition state stabilization by means of electrostatic effects.

1. Introduction

The cytochromes P450 (CYP or P450) form a superfamily of heme-enzymes, which are made up by a large number of isoforms, and they are responsible for the oxidative metabolism of a broad variety of substrates, both endogenous and exogenous.[1-2] These enzymes have the ability to activate dioxygen by means of their prosthetic group, an iron-heme porphyrin, in order to catalyze the oxidation of unactivated hydrocarbons. In this way, P450 uses molecular oxygen to insert an oxygen atom into the C-H bond of their substrates, usually as a hydroxyl group, while the other oxygen is reduced to a water molecule.[3-6] This process is known as monooxygenase reaction (that is the reason why P450s are called monooxygenases), and requires both molecular oxygen and NADPH as co-substrates.

Human Aromatase (CYP19A1) is an isoform of this superfamily and is located in different tissues such as gonads, adrenal glands, ovaries, testes, placenta, ovaries, adipose tissue and in the brain.[7-8] This enzyme, also known as estrogen biosynthetase, is responsible for the last (and key) step of the biosynthesis of steroid hormones from cholesterol. Specifically, aromatase is involved in the formation of C_{18}-estrogens: estrone (E1), 17β-estradiol (E2) and 17β,16α-estriol (E3), from the C_{19}-androgens: androstenedione (ASD), testosterone (TST) and 16α-hydroxytestosterone (HTST), respectively.[9-10] In fact, this is the only known enzyme involved in the biosynthesis of estrogens from androgens in vertebrates.[11] This conversion consists of the aromatization of the A ring of the androgens, which occurs through a process of three consecutive oxidations of the angular C_{19}-methyl group of the androgens.[12-16] In this catalytic process, each oxidation step consumes one mol of NADPH, one mol of molecular oxygen and requires of the presence of the cytochrome P450 reductase (CPR) as a source of electrons.[10, 17-22] The overall process of aromatization of androgens via the enzyme aromatase has been depicted in Scheme 1.

As can be observed in this scheme, the first and the second oxidation steps occur through two consecutive hydroxylations of the C_{19}-methyl group of the androgen substrates. The first step produces 19-hydroxy-androgens, while the second one leads to the formation of the 19-gem-diol species; the latter, is then dehydrated to the aldehyde intermediate (19-oxo-androgen). Finally, the third step consists of a lyase reaction, in which the C_{10}-C_{19} bond of the androgens is cleaved, resulting in the aromatization of the phenolic A ring of the androgens, and expelling formic acid and a water molecule. The literature on this mechanism is very extensive since it has been studied by means of both experimental [12-15, 23-31] and theoretical techniques.[32-39] However, the third oxidation step is still under discussion, in which has not yet reached a consensus. It must be noted that the purpose of this scientific paper is out of participating in this debate.

As mentioned above, the first of the three consecutive oxydation steps of estrogens formation consists of the hydroxylation of the androgens to form 19-hydroxy-androgens. As can be seen in Scheme 2, this process proceeds through two distinct stages: Initially, a C-H bond of the C_{19} methyl group of the androgens is activated by means of the reactive species, an iron(IV) oxo-porphyrin cation radical also known as “Compound I” (Cpd I),

which subsequently abstracts the hydrogen atom to the substrate. In this way, an alkyl radical is generated on the C_{19}-methyl group and the iron-hydroxo porphyrin complex is formed. Later, a reorientation of both the alkyl and OH groups is produced to facilitate the subsequent oxygen rebound step in which a new C-O bond is formed. In this step, the alkyl radical is recombined with the iron-bound hydroxyl radical to form the corresponding hydroxylated substrate and the iron(III) porphyrin complex.

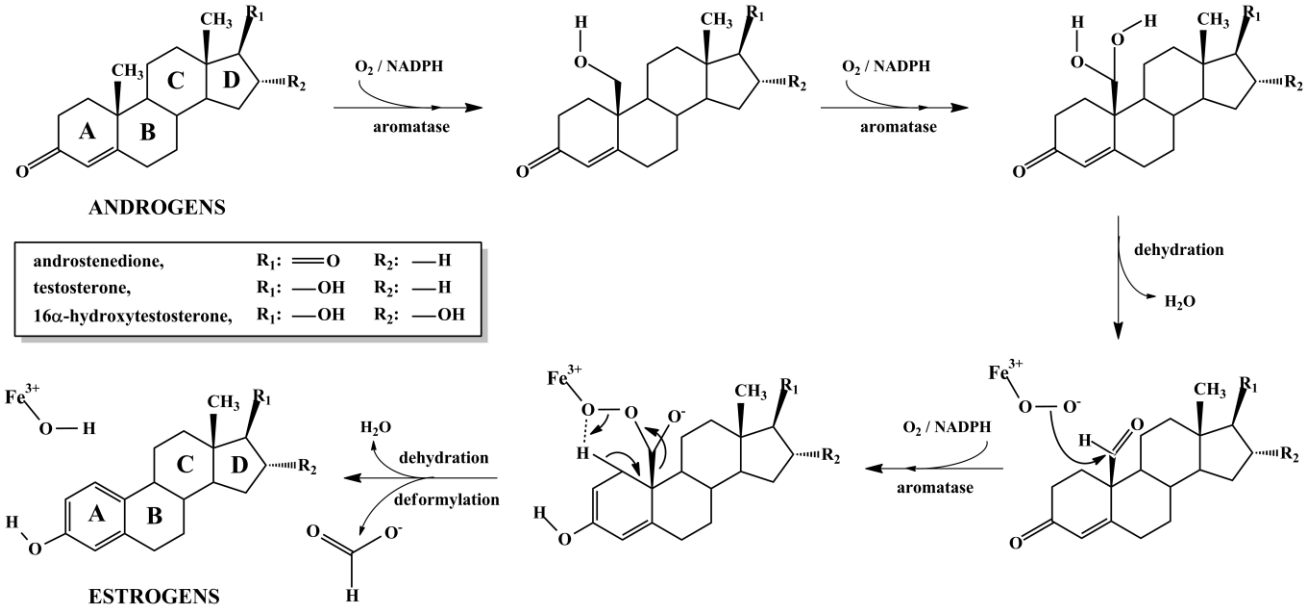

Scheme 1. Proposed catalytic cycle for the aromatization of androgens into estrogens via the enzyme aromatase (CYP19A1).

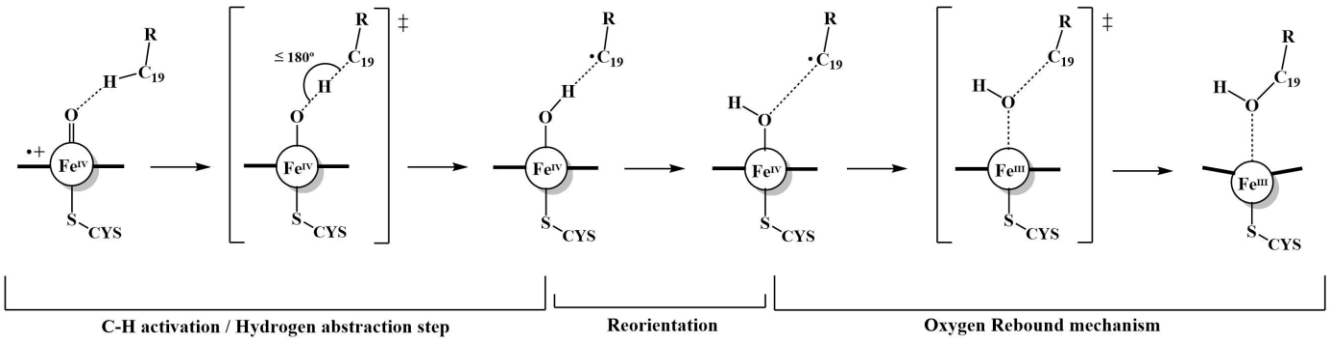

Scheme 2: Mechanism of hydroxylation by cytochrome P450.

Recently, the hydroxylation of the androgen ASD to 19-hydroxy-ASD via the enzyme aromatase was studied by our research group, using hybrid quantum mechanics/molecular mechanics (QM/MM) techniques.[40] According to our findings, the mechanism discussed above, which is common for all cytochromes P450, is fully compatible with the androgen hydroxylation by aromatase enzyme. In this work, apart from calculating the free energy of the whole hydroxylation mechanism, an analysis of the decomposition of the interaction energy for substrate and cofactor was performed. This analysis revealed that the role of the enzyme aromatase during this catalytic subcycle consists of the TS stabilization achieved through both dispersive and polarization effects.

The estrogens are important in humans because of the role they play in the sexual and reproductive development. Particularly the estrogens are essential for women, since these are the primary female sex hormones. In premenopausal women, the main source of estrogens is the ovary, which produces mostly E1. However, in postmenopausal women the source of estrogen production is attributed to the aromatization of adrenal and ovarian androgens (ASD and TST) to estrogens (E1 and E2) via the enzyme aromatase in peripheral tissues.[41] These steroid hormones, apart from being essential in the female sexual development, also play a significant role in the growth and proliferation of hormone-dependent breast cancer. This is because the estrogens bind to the estrogen receptor (ER), which activates the transcription of its target genes, thereby stimulating proliferation of human mammary cells. The complex estrogen-ER interacts with the DNA and may cause mutations due to the resulting increase in cell division, thus encouraging the development of breast cancer cells.[42-43] Around two thirds of all cases of breast cancer are related with the type of hormone-dependent breast cancer,[44-46] however, this ratio is increased up to 75% when we refer to postmenopausal breast cancer.[47] For this reason, blocking the estrogen biosynthesis has proved to be a good strategy to combat the estrogen-dependent breast cancers, and has been a prime goal in the field of endocrinology. Therefore, inhibition of the enzyme aromatase, by means of drugs known as aromatase inhibitors (AIs), is the frontline therapy for these types of cancers.[10, 44, 48]

The AIs can be classified, according to their structures into Type I (steroidal) and Type II (nonsteroidal) inhibitors.[49-50] The former, such as exemestane (EXE) or formestane, have similar structure to natural substrate ASD and hence they act as pseudo substrates of aromatase. In such a way, these inhibitors irreversibly bind the enzyme active site and thus are considered as a mechanism-based inactivators or suicidal inhibitors. The latter, are mostly azole-based compounds, such as anastrozole or letrozole, which are triazole derivatives. These inhibitors compete reversibly with the natural substrate for binding the enzyme, thus interfering with the heme-iron moiety of the cofactor.[41, 43, 51-52] Currently the first-line therapy for advanced hormone dependent breast cancer is based on the third generation of AIs. This family of inhibitors consists of three compounds: anastrozole, letrozole and exemestane, which are marketed under the brand names ARIMIDEX®, FEMARA® and AROMASIN® respectively.[41, 48]

In recent times, the aromatase inhibition has been studied by means of different computational techniques, where several AIs have been tested.[10, 43, 51, 53-57] In this paper, we have focused in particular on the EXE compound (6-methylene-androsta-1,4-diene-3,17-dione) because of the resemblance it has with the natural substrate ASD (androst-4-ene-3,17-dione). EXE shares the steroidal backbone with ASD, however, the main differences that

exist between them are: i) a C_6-substitued methylidene group located at the B-ring of EXE, and ii) a double bond between C_1 and C_2 carbons which is present at the A-ring of the EXE but not in the ASD (see Scheme 3 for comparison).

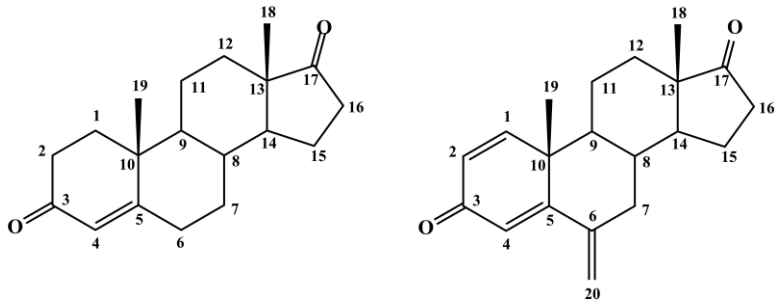

Scheme 3: Structure of the androstenedione and exemestane substrates.

On one hand, the ability to block enzyme activity by the exemestane has been attributed to the presence of this C_1-C_2 double bond.[41, 58] On the other hand, it has been reported that the presence of the C_6-methylidene improves the binding of the EXE in the active site, by means of a "hydrophobic clamp" comprised by the residues Thr-310, Val-370 and Ser-478.[10] In this way, the tight interaction between the C_6-methylidene and the hydrophobic crevice might reduce the mobility of the Thr-310, thus interfering with the mechanism of formation of the Cpd I (in the absence of CPR), and not being the EXE hydroxylated.[10-11]

Given the structural characteristics of EXE, it seems reasonable to assume that it shares the catalytic cycle with the natural substrate (ASD), at least in its early stages. Therefore, we have performed a theoretical QM/MM study of the hydroxylation of EXE substrate to 19-hydroxy-EXE catalyzed by the enzyme aromatase, with the aim of comparing this mechanism with which occurs during the first catalytic subcycle of the enzyme. With the present work, we attempt to address the following questions: (i) Is the hydroxylation of EXE compatible with that observed for the ASD, in terms of activation energy? (ii) Does the suicidal inhibition take place in this mechanistic step? (iii) How does the hydrophobic cleft affect to the activation energy of the process?

2. Computational Methods

System Setup

The X-ray crystal structure of the human placental aromatase cytochrome P450, in complex with its natural substrate ASD (PDB code 3EQM),[11] was used as the startup geometry in our simulations. The heme cofactor

existing in the original PDB file was altered to obtain the Iron-Oxo porphyrin Cpd I species, according to the atomic positions suggested in the literature.[11] In addition, the substrate ASD accommodated in the active site of aromatase was modeled to EXE, being the latter retained in the same position than the crystallized ASD. To this end, a methylidene group (*=CH_2) was substituted in the C_6 carbon and the single bond between positions C_1 and C_2 was modified to a double bond. All the hydrogen atoms were added using the fDYNAMO library,[59] according to the pKa values rendered by the empirical propKa program.[60] Standard protonation states in solution were found with the exception of the residue Asp-309, which was protonated at pH 7, given that it exhibited a large pKa displacement (7.7). Histidine amino acids were protonated as follows: His-(62, 105, 111, 325 and 475) were singly protonated at ε position, His-(109, 128, 402, 459 and 480) were singly protonated at δ position and His-171 was doubly protonated. A total of 3 counter ions (Cl^-) were accommodated into optimal electrostatic positions with the aim of electroneutralize the system. The model was placed in a orthorhombic box of water molecules of 90x80x80 Å, erasing any water molecule whose oxygen atom lies less than 2.8 Å from any heteroatom. The resulting model consisted of 452 residues of amino acids, the Cpd I, the substrate EXE as well as 35 crystallographic water molecules, 3 counterions and 16553 water molecules of the solvation box.

A QM/MM relaxation of the resulting model was accomplished, using the L-BFGS[61] algorithm. With this purpose, the substrate molecule was described using the AM1[62] semiempirical Hamiltonian, while the enzyme, the Cpd I and the counterions were described classically in terms of the OPLS-AA[63] force field. All the water molecules, including the crystallographic ones, were treated using the TIP3P[64] water potential. Finally, the equilibration of the resulting structure was performed by means of hybrid molecular dynamics (MD) at 300 K, using the Langevin–Verlet integrator and under the NVT ensemble. The MD was run for 200 picoseconds (ps) with a step size of 1 femtosecond (fs). The nonbonding interactions were applied in the calculations by means of periodic boundary conditions with the minimum image convention, using a force-switch function with a cutoff distance in the range 14.5-16 Å.

QM/MM Calculations

In order to study the reactivity of the enzyme aromatase with the substrate EXE, the potential energy surfaces (PES) were explored by means of QM/MM calculations. The strategy used to localize the TSs during the QM/MM calculations was the micro/macroiteration method.[65] In this method, the full system is divided into two different subgroups: the control space, consisting of the atoms participating in the reaction, which are treated by means of quantum methods, and the complementary space that includes the rest of the system. In this way, the optimization of the system is performed as a combination of iterations in both subgroups, which allows taking advantage of efficient optimization algorithms. For each optimization step of the control space (based on the Baker[66-67] algorithm), the complementary space remains completely relaxed (using the L-BFGS algorithm). Since the complementary space optimization (macroiterations) usually demands a large number of gradient calculations for each optimization step of the control space (microiteration), a dual QM:Charge/MM scheme[65, 68]

was adopted. In this procedure, the QM/MM potential energy of the system is evaluated using different expressions, depending on the coordinate space being optimized. In this way, the QM atoms are represented as frozen classical charges throughout the macroiterations, which accelerates the calculations. In addition, due to the complexity of the system, a truncation scheme was carried out during all the QM/MM simulations. Therefore, a list of interactions (comprising all atoms within 20 Å from both the Cpd I and the substrate EXE) is defined at the beginning of the simulations and is held constant during all of them. In such a way, all the residues further than this distance remained frozen during the simulations while all the residues included in the list were allowed to move.

Once the TSs were obtained and characterized, minimum energy paths (MEP) were mapped out in order to obtain all the stationary points involved in the reaction. Then, the Gibbs free energy was computed on these stationary points, under the rigid-rotor and the harmonic-oscillator (RRHO) approximations, taking into account both thermal corrections and zero point energy (ZPE).

The QM region of the model consisted of 123 atoms distributed among the EXE substrate, the Cpd I and the axial Cys-437 ligand (comprising the S_γ, the C_β and two H_β atoms), as can be seen in Figure 1.

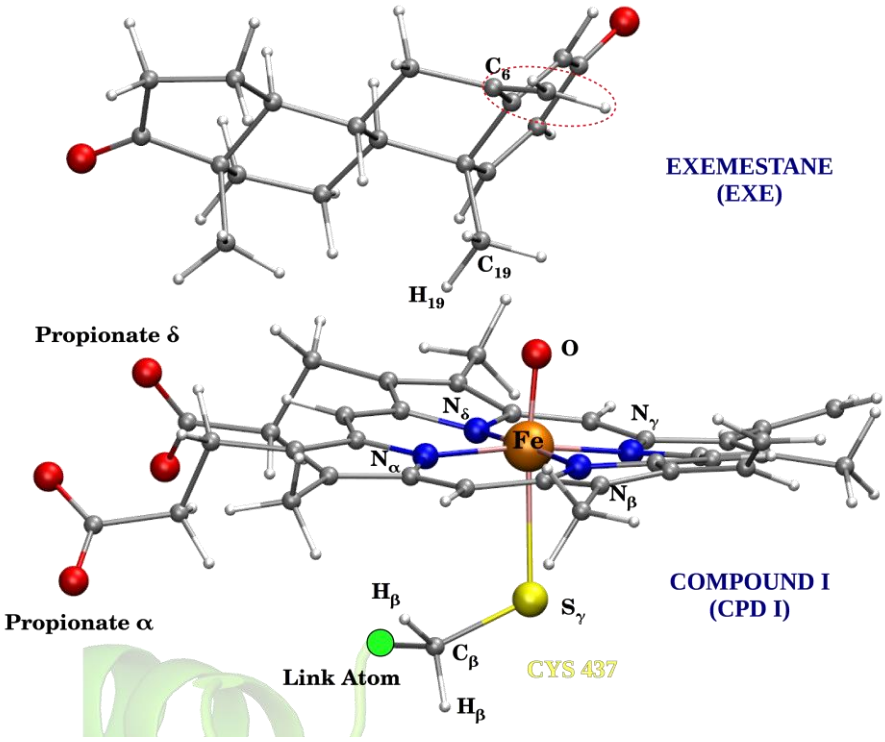

Figure 1. Atoms belonging to the QM model: Cys-437 residue, the substrate EXE and the cofactor Cpd I. The C_6-methylidene of the exemestane has been highlighted with a red dashed line.

The quantum atoms belonging to the QM region were described by means of the LACVP* basis set[69] (named as B1), where the 6-31G(d) basis is used to describe all the atoms except the iron, which is represented by the

Lanl2dz effective core potential (ECP). Additionally, with the aim of calculate a more precise energies and frequency numbers, single-point calculations were performed using a larger basis set (B2) on the stationary points previously located with the B1 basis set. The new B2 basis set consists of the combination of the Lanl2tz+ ECP for the iron and the 6-311G(d,p) basis for the rest of the atoms. The level of theory employed during the QM calculations was the unrestricted Kohn-Sham formalism with the B3LYP[70-71] density functional. The DFT and DFT/MM methodologies have been reported to adequately describe the ground states of both the doublet and the quartet for the Cpd I.[72-73] In fact, B3LYP has become the widely accepted choice to treat the quantum calculations of the CYP enzymes, since it is well-known that this functional provides reasonable relative spin state energies as well as a number of other properties.[74-75] As in the system setup, the rest of the enzyme as well as the water molecules (MM region) were described classically by means of the OPLS-AA and TIP3P force fields, respectively. In addition, the link atom formalism was adopted to satisfy the valence of the QM region, due to existence of a classical bond partitioning in the Cys-437 amino acid (C_α-C_β bond). All the DFT calculations were carried out using the Gaussian03[76] program, while the MD simulations and the MM calculations were performed with the fDYNAMO library.

Free energy perturbation calculations

In order to compute the free energies of activation of this enzymatic reaction, free energy perturbation (FEP) calculations were performed on the system. Since this method is based on statistical mechanics, the conformational space of the enzyme is taken into account in the calculations, thereby allowing us to obtain more accurate free energy surfaces. With this purpose, a series of windows (geometries with equally spaced energy) were chosen from the formerly mapped out reaction paths. Specifically, 67 windows were selected for the doublet spin state and 76 for the quartet state. During the FEP calculations, the QM region (including the link atom) of each window remained frozen. Every time a QM energy calculation was performed, 100 steps of classical MD were carried out (following the micro/macro scheme), under the same conditions used during the equilibration. This scheme was applied 200 times with a time step of 1 fs, giving rise to a total of 20 ps per window. Finally, in order to estimate the variation of free energy change, the coordinates of the QM region were shifted between consecutive windows (for the last 100 structures), using the following expression:

$$\Delta F_{i\to j} = -RT \ln \langle e^{-\left(\frac{H_j - H_i}{RT}\right)} \rangle_i \qquad (1)$$

This equation is expressed as an average of potential QM/MM energy differences as denote the triangular brackets. The term H_i refers to the potential energy of the i_{th} window of MD, meanwhile H_j corresponds to the potential energy calculated after swapping the coordinates of the atoms of the control space (j=i+1 for forward or j=i-1 for backwards). The average was carried out under the same geometry of the classical environment

corresponding to the i_{th} window. Once the free energy barrier is computed using this equation, the ZPE correction term is added by means of QM/MM frequency calculations, performed on both the reactant and TS structures.

3. Results and Discussion

The results presented in this paper correspond to the hydroxylation of EXE substrate to 19-hydroxy-EXE catalyzed via the enzyme aromatase. This process is divided in two stages: an initial hydrogen abstraction process and a subsequent oxygen rebound step. At first, the reaction was studied at the active site of the enzyme in the doublet spin state, using the B3LYP[B1]:ESP/MM scheme discussed above. Then, the search of the transition states in the quartet state was performed from the optimized structures of the doublet, from which the entire PES was obtained.

Table 1 shows the Gibbs free energies (ΔG) obtained with the B2 basis set for the entire hydroxylation process, as well as the activation free energies obtained from FEP (ΔF) only for the first hydrogen abstraction step. The FEP calculations were carried out with the B1 basis set and afterwards were corrected with the larger basis set B2. However, this correction was only applied to those energy terms that can be extracted from the average. With this purpose, equation 1 was rewritten in order to reduce the large amount of time consuming QM(B2) calculations:

$$\Delta F \approx -RTln\langle e^{-\frac{\Delta E_{Int}^{B1}}{RT}}\rangle + E_{vac}^{B2} + \Delta ZPE^{B2} \quad (2)$$

In Equation 2, the interaction energy term (ΔE_{Int}^{B1}) corresponds to that previously calculated with the B1 basis set, while both the gas phase energy (E_{vac}^{B2}) and the ZPE (ΔZPE^{B2}) terms were estimated with the B2 basis set.

As can be observed in Table 1 and Figure 2, the reactant species show Gibbs free energy values quite similar in both spin states, being the quartet 1.0 kcal/mol lower than the doublet state. The ΔG of activation for the hydrogen abstraction step (the rate-limiting step of the reaction) falls in the range of 18-19 kcal/mol, being in this case lower for the doublet than for the quartet. The intermediates generated in this step correspond with the iron-hydroxo complex and alkyl species and give place to the oxygen rebound process. The ΔG of activation for this step shows values of 1.7 kcal/mol for the doublet and 5.5 kcal/mol for the quartet, leading to the formation of the 19-hydroxy-EXE through a highly exergonic process (-42 and -47 kcal/mol for the doublet and quartet, respectively).

The free energies were also calculated by means of FEP techniques, in order to include the flexibility of the enzymatic environment. The values calculated with this methodology are reported in Table 1 and are depicted in Figure 3. As can be seen in Table 1, the ΔF energies obtained for the reactant species with the B1 basis set are almost degenerate (< 0.5 kcal/mol), being lower in the case of the quartet state. Indeed, when the B2 basis set is

considered, this difference is even lower, being both spin states virtually degenerated. The ΔF of activation for the hydrogen abstraction step obtained with the B1 basis falls in the range of 17-19 kcal/mol, being the barrier of the doublet state lower than for the quartet. However, these barriers decrease to values in the range of 15-18 kcal/mol once the B2 basis has been considered. Interestingly, when the values calculated from PESs (ΔG) are compared with those calculated through FEP techniques (ΔF), it can be noted that the inclusion of the conformational space of the enzyme has not a significant impact on the activation barriers. Surprisingly, this trend is in clear contrast with that observed in a previous investigation including the ASD substrate,[40] where the barriers calculated for the H-abstraction by means of FEP, were about 9 kcal/mol smaller in average than those calculated from the PES. In addition, our results indicate that the hydroxylation step is slower for the EXE than for the natural substrate ASD, since the barrier for the rate-limiting step of the reaction is 3.4 kcal/mol higher for the EXE (16.9 kcal/mol) than for the ASD (13.5 kcal/mol). It is worth mentioning that the ΔF values used in the comparison between both studies are those obtained for the doublet state with the B1 basis set. Indeed, this observation is in good agreement with the values derived from experimental results; specifically when compared to the data obtained from kinetic studies for the hydroxylation of both substrates. According to the kinetic parameters obtained experimentally for the EXE (global rate of $0.83 \cdot 10^{-3}$ s^{-1})[77] the free energy barrier for the entire inhibition process at 310 K is around 22.5 kcal/mol. Moreover, the whole aromatization process of the ASD presents a free energy barrier around 19.8 kcal/mol at the same temperature (experimental global rates of 0.06 s^{-1} and 5.69 min^{-1})[27, 29]. The hydroxylation of ASD is in turn the rate-limiting step of the aromatization, and it is characterised by a free energy barrier of 18.2 kcal/mol (kcat of 1.0 s^{-1})[27]. Under the assumption that the hydroxylation of the EXE is also the rate-limiting step of the catalytic cycle, as is the case of the ASD, the free energy of activation for EXE would be around 2.4 kcal/mol higher than for the ASD. Although our reported activation barriers are underestimated (around 5 kcal/mol) when compared with the experimental values, the difference of the activation barrier that we have obtained between the EXE and ASD falls in the range experimentally observed.

Furthermore, the hydroxylation of EXE is more exergonic than the hydroxylation of ASD (4.8 kcal/mol for the doublet and 3.3 kcal/mol for the quartet state, respectively). This observation suggests that EXE could act as a competitive inhibitor in the first catalytic subcycle of human aromatase.

Table 1. Relative potential energies (ΔE_{pot}) and free energies obtained by means of RRHO (ΔG) and Free Energy Perturbation (ΔF) for the hydroxylation of EXE in doublet and quartet spin states. The FEP energy has been calculated only for the hydrogen abstraction step and the ZPE has been included in both ΔG and ΔF. The

basis set used (B1 or B2) is shown in parenthesis. The energies are expressed in kcal/mol and the imaginary frequencies (cm^{-1}) associated with each TS obtained are also reported.

	ΔE_{pot} (B2)	ΔG (B2)	ΔF (B1)	ΔF (B2)
^2R	1.5	1.0	0.4±0.0	0.0
^4R	0.0	0.0	0.0±0.1	0.2
$^2TS_{H\text{-}abs}$	24.1	18.7 (1764*i*)	17.3±0.1	15.2
$^4TS_{H\text{-}abs}$	24.0	19.1 (1878*i*)	19.2±0.2	17.8
^2I	14.7	11.7	14.5±0.2	10.8
^4I	13.4	10.5	13.3±0.2	9.7
$^2TS_{reb}$	15.6	13.4 (171*i*)		
$^4TS_{reb}$	18.4	16.0 (328*i*)		
^2P	-43.2	-41.7		
^4P	-47.6	-46.7		

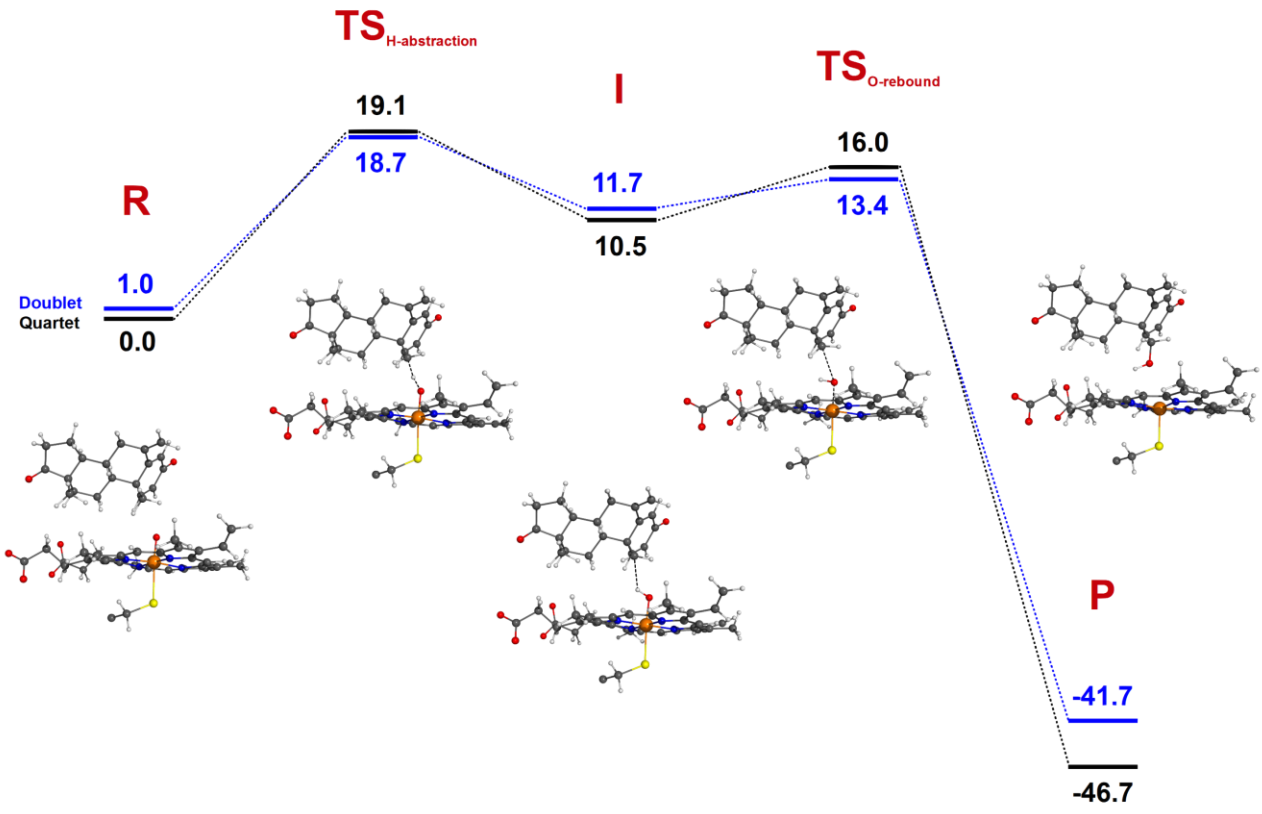

Figure 2. Gibbs Free Energy profile (kcal/mol) for the hydroxylation of the EXE substrate. The structures corresponding to the QM part for each stationary point have been depicted.

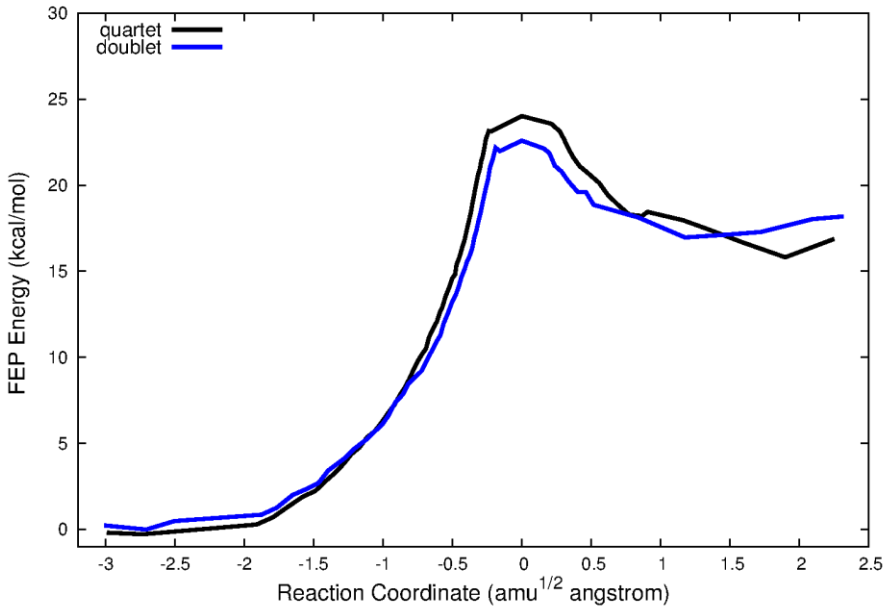

Figure 3. Free Energy profile (kcal/mol) of the hydrogen abstraction step from the EXE substrate. This profile has been obtained by means of FEP techniques using the B1 basis set. The ZPE energy has not been included in the profile.

The reaction process can be monitored through the values of spin density and the geometrical parameters of the structures obtained. The geometrical data obtained for the hydroxylation of EXE and the corresponding Mulliken atomic spin densities using the B2 basis set are reported in Tables S1 and S2 of the Supporting Information, respectively. Moreover, the evolution of the molecular orbitals occupancy along the hydroxylation process, for doublet and quartet states, has been depicted in Figure 4.

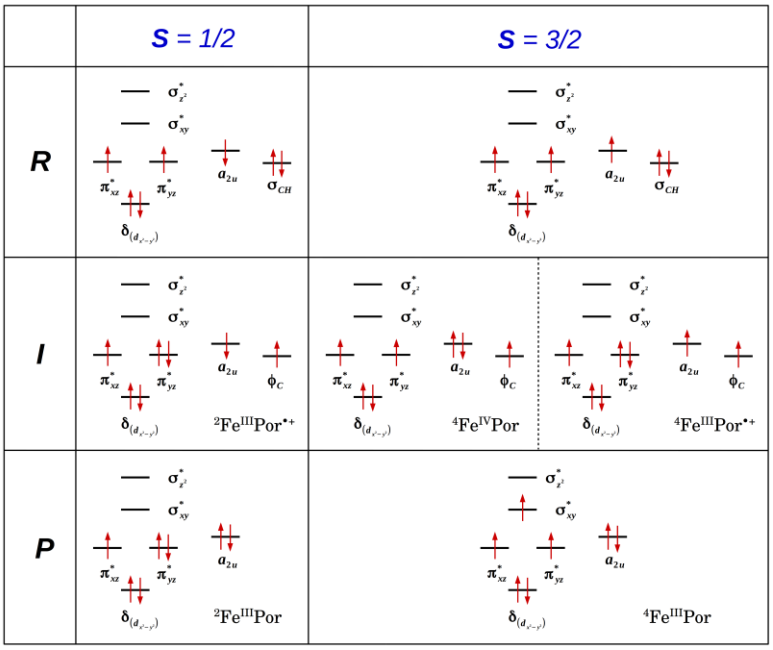

Figure 4. Evolution of the molecular orbitals occupancy along the hydroxylation of the EXE substrate, for doublet (S=1/2) and quartet (S=3/2) spin states.

As can be observed in Figure 4 and in Table S2, the reactant species concentrate the entire spin density on the FeO moiety (local triplet) and on the a2u orbital of the porphyrin ring: (ρ(FeO)=2.12, ρ(Por+SCH_3^-)=-1.12) for doublet and (ρ(FeO)=2.04, ρ(Por+SCH_3^-)= 0.96) for quartet. Inasmuch the hydrogen abstraction takes place, the H_{19} atom along with the unpaired electron coming from the homolytic C-H cleavage are transferred from the C_{19} to the oxygen of the Cpd I. During this process, the Fe-O bond is stretched (from ~1.6 Å to ~1.8 Å), while the Fe-S distance is slightly contracted (from ~2.6 Å to ~2.5 Å). At the same time, the distance between the donor (C_{19}) and the acceptor (O) atoms becomes shorter when going from the reactive species to the transition structures (from 2.9 Å to 2.5 Å). It is noteworthy that the TS shows the maximum value of the angle C_{19}-H_{19}-O (~168 degrees), which is a value close to linearity, as expected for this type of hydrogen transfer mechanisms. However, the O-C_{19} distance again elongates as the formation of intermediate species occurs, thus taking similar values to those of the reactants (~2.9 Å). This step leads to the formation of an alkyl radical on this carbon (ρ(C_{19})~1.00) and of the iron-hydroxo complex (ρ(O-H_{19})<0.20) in the intermediate species. Interestingly, the iron-hydroxo complex was found in two different electromeric configurations for the quartet spin state as can be seen in Figure 4: $^4Fe^{III}Por^{\bullet+}$ (ρ(Fe)=0.90, ρ(Por+SCH_3^-)=0.96) and $^4Fe^{IV}Por$ (ρ(Fe)=2.00, ρ(Por+SCH_3^-)=-0.17). Both electromers share the same geometry, but differ in the occupancy of their molecular orbitals.[75, 78] However, in the case of the doublet state, only the configuration corresponding to $^2Fe^{III}Por^{\bullet+}$ was found (ρ(Fe)=1.00 and ρ(Por+SCH3$^-$)=-1.08). It is worth pointing that despite of the fact that different electromers were found in the iron-hydroxo complex, all the configurations present in the intermediate species retain the radical character on

the C_{19} atom with a singly occupied orbital Φ_c ($\rho(C_{19})$= 1.00 ($^2Fe^{III}Por^{\bullet+}$), 1.03 ($^4Fe^{III}Por^{\bullet+}$), and 1.03 ($^4Fe^{IV}Por$)). The subsequent rebound step is preceded by a reorientation of the hydroxyl group, which is being prepared to form a new C_{19}-O bond. This rotation process can be monitored through the change in the H_{19}-O-Fe-N_α dihedral angle between the intermediate and the TS of the rebound step (around 55º for doublet and 45º for quartet). The rebinding of the hydroxyl group involves the shortening of the C_{19}-O bond (from ~3.0 Å to ~2.6 Å in doublet and from ~3.0 Å to ~2.5 Å in quartet). This distance, in turn, decreases drastically from the TS to product species (~1.4 Å) giving place to the formation of the new C_{19}-O bond as well as the penta-coordinated iron complex. During the rebound step, the radical character on C_{19} disappears leading to product species showing a closed shell porphyrin as well as unpaired electrons on the Fe(III) center: three in the quartet state and one in the doublet state (see Figure 4). All the spin density found in the products is concentrated on the iron atom (ρ(Fe)=2.69 and 1.30 for quartet and doublet, respectively) and partly in the porphyrin and the thiolate ligand ($\rho(Por+SCH_3^-)$=0.31 and -0.33 for quartet and doublet, respectively).

The main interactions established among the EXE and the Cpd I with the surrounding amino acids of the active site are presented in Figures 5 and 6, and Table S1 of Supporting Information. As can be observed in Figure 5, there are several hydrogen bonds established among the propionate side chains attached to the heme group and the following residues: Arg (115, 145, 375 and 435) and Trp-141. These interactions are responsible for the efficient binding of the heme group in the active site, since they neutralize the excess of negative charge present in the heme-propionate side chains. Similarly, the residues: Ala-438, Gly-439 and Lys-440 stabilize the sulfur atom of the Cys-437, which is partially charged, by means of the interaction with three polar peptidic hydrogens. It has been reported that this interaction stabilizes the coordination of the thiolate with the heme group, and at the same time regulates the redox potential of the heme group, so that prevents the formation of a radical on the sulfur atom.[79]

Regarding the interactions of the EXE substrate, it is noteworthy that it is enclosed in a mainly hydrophobic cleft formed by the residues: Ile-133 and Phe-134 from B-C loop, Phe-221 and Trp-224 from F-helix, Ile-305, Ala-306, Asp-309 and Thr-310 from I-helix, Val-369, Val-370, Leu-372 and Val-373 from the K-β3 loop, Met-374 from β3, Leu-477 and Ser-478 from the β8-β9 loop. EXE in turn forms two hydrogen bonds between its polar moieties (3-keto and 17-keto oxygens) and the residues Asp-309 (which is protonated) and Met-374, respectively. Some of the interactions discussed above can be seen in Figure 5.

When comparing the interactions between the EXE and ASD substrates with the active site of aromatase, we see that the main difference lies in the interactions between the substituted C_6 carbon and its nearest surrounding amino acids. It should be remembered that both substrates differ in the functional group substituted on C_6, which is located in a quite exposed position, due to its proximity to the access channel to the aromatase active site. The EXE substrate has a methylidene group substituted in this position that makes it bulkiest than the same position in the ASD (which is not substituted), and hence it has more surface accessible to fit in the available space. A study based on docking techniques[10] has proposed the existence of a "hydrophobic clamp" in the active site,

which comprise the residues Thr-310, Val-370 and Ser-478, and that it would be responsible for anchoring the C_6-methylidene of EXE, thus improving the binding of the inhibitor.

In our simulations, we have observed that the C_6-methylidene interacts with the residues Phe-221, Thr-310, Ser-478, Val-369, Val-370 and a water molecule (WM) (see Figure 6). The distances among the main atoms of the residues described above and the C_{20} atom of the EXE range from 3.2 Å to 4.9 Å (see Table S1 of the supporting information). Interestingly, we have observed a bridge of polar nature formed by the peptide carbonyl group of Asp-309, the WM, and the Hγ of the Ser-478, which is located in the vicinity of the access channel. This polar bridge is aligned with the methylidene group and would provide a binding region of electrostatic nature. It should be pointed out that we have observed the presence of a conformer of the Thr-310 residue, in which the Oγ1 hydroxyl moiety is located between the residue EXE and the heme group. The orientation of this residue also reveals an interaction of the Oγ1 atom with a C_{19}-methyl hydrogen of the EXE substrate, whose average value is 2.7 Å (see Figure 5). Based on the short distance between both atoms (<2.9 Å), one could think that this interaction assists the orientation of the C_{19} atom, thus facilitating the hydrogen abstraction process. It is worth pointing that this disposition differs from that found in the original X-ray structure, in which the Cγ2 is located between the substrate and the heme group. However, it is necessary to mention that during the calculations that we performed with the ASD substrate, the orientation of Thr-310 was retained in the same position than in the original structure from X-ray. In order to check how stable the Thr-310 rotamer is, classical MD simulations were carried out for two different conformations: (a) the one obtained from the analysis of the PES, and (b) another one in which the Thr-310 was modified with the aim of reproducing the orientation found in the X-ray structure. Each MD was run for 30 nanoseconds (ns) with the program NAMD[80] with a step size of 1 fs using the TIP3P water model and the OPLS-AA force field. The results of the MD calculations showed that the orientation of the Thr-310 remains unaltered in each of the simulations, which suggests that the two rotamers are representative of the conformational space of the protein. Indeed, the distance between the Oγ1 atom and the C_{19}-methyl hydrogen of the EXE substrate shows an average value of 3.1±0.4 Å for the conformer (a), while this value is 4.9±0.3 Å for the conformer (b). On another note, the conformer (a) shows an average potential energy lower than the conformer (b); specifically, this energy is ~146 kcal/mol more negative in (a) than in (b) for the last 1000 structures analyzed (see Figure S1 of the Supporting Information for more detail). Moreover, the activation energy for the hydrogen abstraction step was also calculated (with the B1 basis set) in the case of the conformer (b), giving place to a free energy barrier 3.5 kcal/mol higher than for the conformer (a). Further details regarding the energies and structures obtained in these calculations can be seen in the Table S3 and Figure S2 of the Supporting Information.

Furthermore, the stability of the polar bridge, which was discussed above, was also checked from the MD simulations. Based on the analysis of 30,000 structures, we observed that this bridge is only present in around 7% of the time of simulation. This finding can be partly explained by the fact that the residues involved in the bridge are found in a region quite exposed to solvent, and therefore, the water molecules are free to come in and go out through the access channel. Indeed, the Hγ1 atom belonging to the Ser-478 residue establishes hydrogen

bonds with the peptide carbonyl group of the residues: Ser-478, Val-369 and Asp-309, and with the Nε atom of the residue His-480. In any case, this polar bridge would introduce certain electrostatic character to the interaction between the methylidene group and the active site.

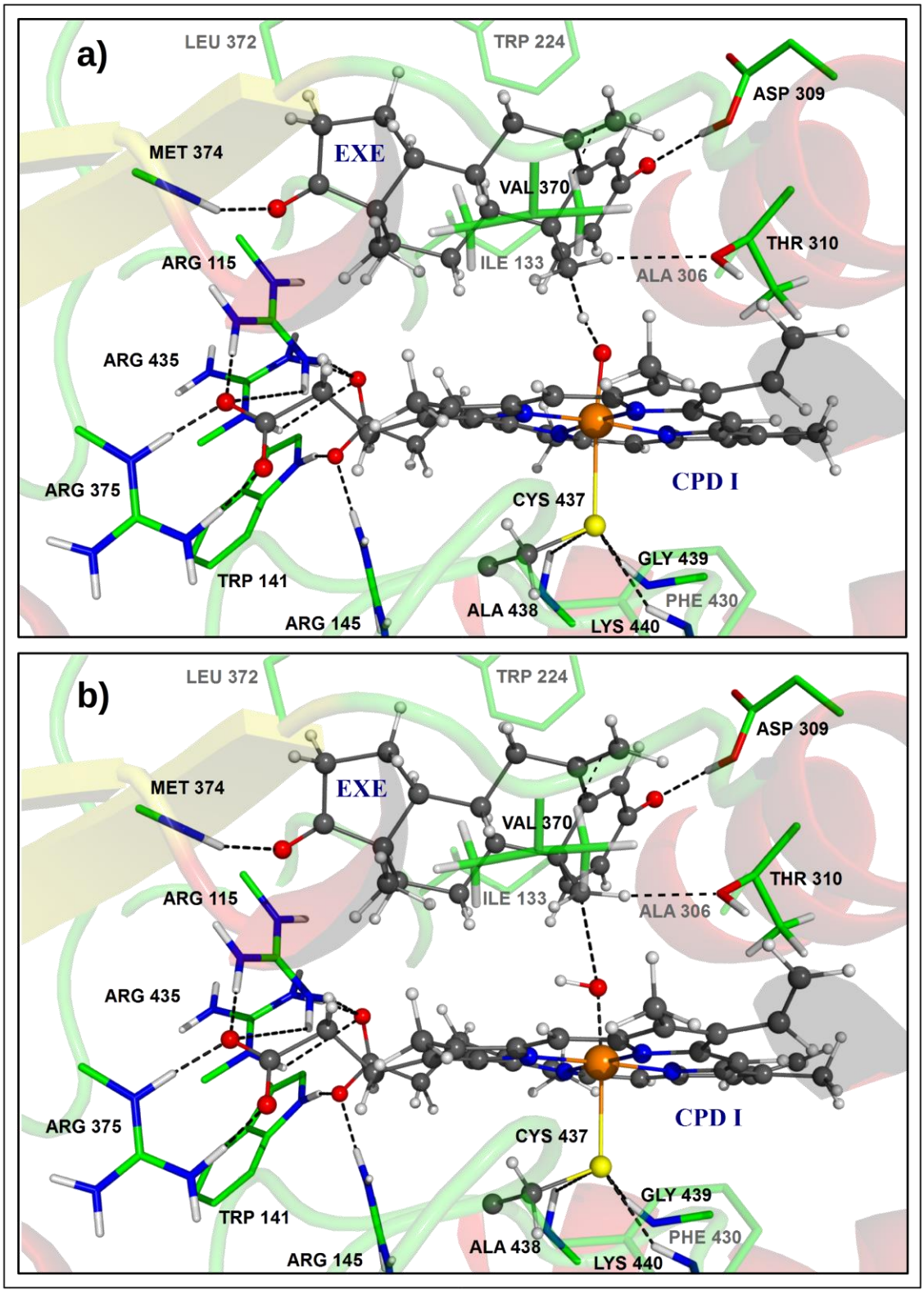

Figure 5. Snapshots corresponding to the TS structures obtained during the hydroxylation reaction of the EXE substrate: (a) for the hydrogen abstraction and (b) for the oxygen rebound step. The most relevant interactions among the substrate and the cofactor with the enzymatic environment have been depicted.

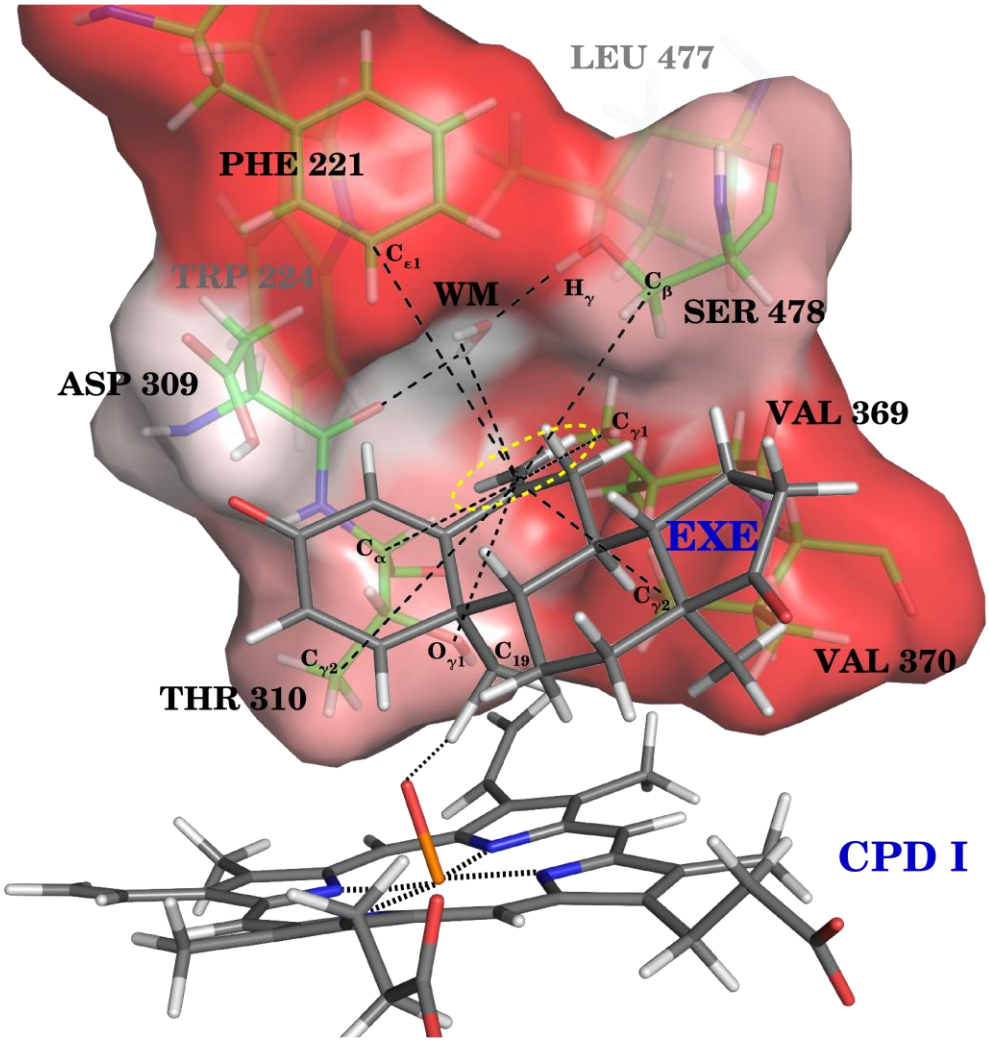

Figure 6. Representation of the main interactions of the C_6-methylidene group (highlighted in yellow dashed lines) with the surrounding amino acids. Notice that WM means water molecule. The solvent accessible surface in the vicinity of the methylidene group has been depicted and it has been colored according to the hydrophobicity (white for the polar interactions and red for hydrophobic interactions).

Finally, the interaction energy between the enzymatic environment and the substrate/cofactor was calculated for the hydrogen abstraction step (rate limiting step) in both doublet and quartet spin states. This energy was obtained from the FEP windows corresponding to reactant and TS structures, and thus is expressed as an average value. Moreover, in order to unravel the source of the catalytic activity of aromatase during the chemical process, the interaction energy was further broken down into its constituent parts. Table 2 shows the results

obtained for the different contributions of the interaction energy, which are as follows: i) the electrostatic term (ΔE_{elec}), which corresponds to the interaction between the polarized wave function obtained for the substrate/cofactor and the MM charges representing the enzymatic environment; ii) the polarization energy (ΔE_{pol}), consisting of the energy associated with the deformation of the wave function obtained in gas-phase, when it is perturbed by the effect of including the enzyme environment; iii) the Lennard-Jones term (ΔE_{LJ}), representing the classical dispersive interaction between the QM and MM atoms. This interaction has been in turn broken down into the contributions coming from the atoms of the substrate (EXE) and from the cofactor (Cys+heme). Additionally, the gas-phase energy (ΔE_{vac}) obtained for each species is also presented in Table 2.

Our results reveal that the electrostatic interaction term is the only responsible for the TS stabilization with respect to the reactant species, being ΔE_{elec} = -14.5 and -3.2 kcal/mol for the doublet and quartet, respectively. In contrast, it is observed that both the polarization and the Lennard-Jones terms lead to an unfavorable contribution to the activation energy. However, these contributions have different weight depending on the spin state being monitored, in such a way that ΔE_{pol} and ΔE_{LJ} show values of 4.0 and 7.9 kcal/mol in the case of the doublet, which are higher than those obtained in the case of the quartet (0.8 and 0.2 kcal/mol, respectively). In addition, when the ΔE_{LJ} energy is decomposed in terms of substrate (ΔE_{LJ} (EXE)) and cofactor (ΔE_{LJ} (Cys+heme)), a different trend is also noted depending on the spin state. Interestingly, the latter gives rise to a destabilizing nature in the case of the doublet (6.5 kcal/mol), but slightly stabilizer in the case of the quartet state (-0.8 kcal/mol). Nevertheless, despite the fact that the different contributions to the activation energy for the doublet state are higher in magnitude than for the quartet, the global interaction energy of the activation process (the sum of all the different contributions), falls into the same range for both the doublet (-2.6 kcal/mol) and the quartet (-2.3 kcal/mol).

Surprisingly, in a previous study that we performed on the same enzyme but with the natural substrate (ASD),[40] we showed that the stabilization of the transition state for the hydrogen abstraction step is achieved by means of Lennard-Jones and polarization effects. Since both substrates share the same steroidal backbone, it would be expected a similar behavior in this regard; however, in present study we observe that the electrostatic term is the only one that facilitates the binding of the transition state in the EXE substrate. In order to better clarify the source of this preferential electrostatic stabilization, we performed a decomposition "residue by residue" of the electrostatic interaction term (ΔE_{elec}) involved in the activation energy. The results obtained are plotted in the Figure 7, and reveal that the residue Thr-310 participates in the stabilization of the TS. These findings suggest that the changing nature of the TS stabilization for the hydrogen abstraction step between both substrates is due to: i) the presence of a methylidene group substituted in the C_6 of the EXE substrate and ii) the different orientation of the residue Thr-310 during the chemical reaction, which forms a hydrogen bond ($O\gamma 1$-H_{19}) with the EXE substrate.

Table 2. Relative QM/MM energy decomposition terms for the hydrogen abstraction (rate-limiting step). The absolute values, along with the corresponding errors, are shown in brackets. The Lennard-Jones term has been in turn broken down into substrate (EXE) and cofactor (Cys+heme), and the gas-phase energies (ΔEvac) have been also included. All the values are expressed in kcal/mol.

	ΔE_{elec}		ΔE_{pol}		ΔE_{LJ}		ΔE_{LJ} (EXE)	ΔE_{LJ} (Cys+heme)	ΔE_{vac}
^{2}R	[-577.8±9.6]	0.0	[60.8±1.6]	0.0	[346.5±10.4]	0.0	0.0	0.0	0.0
^{2}TS	[-592.3±10.5]	-14.5	[64.8±2.2]	4.0	[338.6±11.4]	7.9	1.4	6.5	25.4
^{4}R	[-576.1±9.0]	1.7	[60.5±1.6]	-0.4	[348.8±10.4]	-2.4	1.1	-3.5	-0.6
^{4}TS	[-579.3±11.1]	-1.5	[61.2±2.0]	0.4	[348.7±11.7]	-2.2	2.1	-4.3	25.9

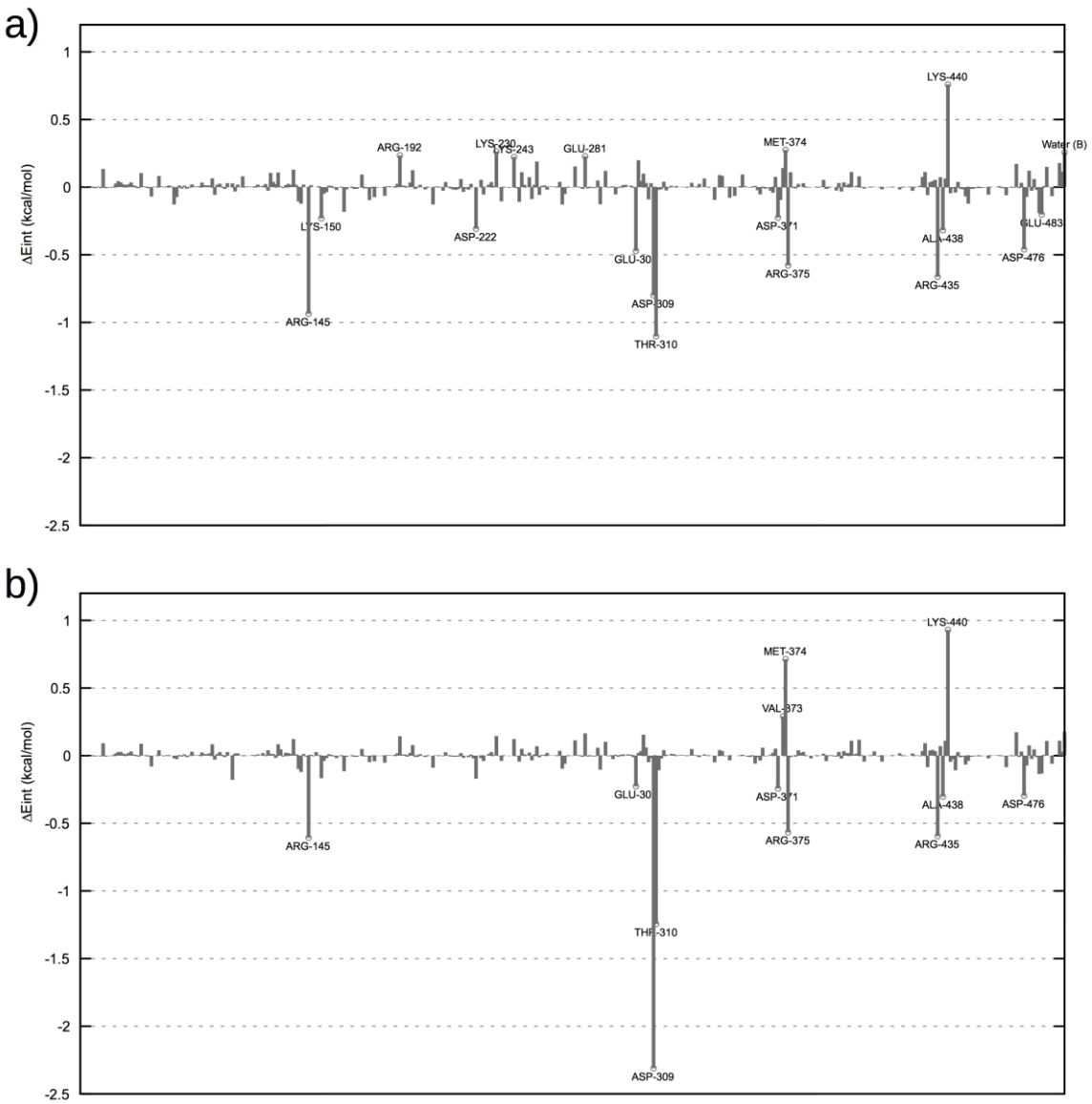

Figure 7. Decomposition "residue by residue" of the activation energy for the electrostatic interaction term (ΔE_{elec}) obtained for the doublet (a) and the quartet (b) spin states. Notice that only those residues contributing with an absolute value greater than 0.2 kcal/mol are labeled in the charts.

4. Conclusions

In the present work, the hydroxylation of the EXE substrate to 19-hydroxy-EXE, catalyzed by the enzyme aromatase, has been studied using hybrid QM/MM calculations and MD simulations. The aim of this study has been to compare the hydroxylation mechanism of this aromatase inhibitor, with that which occurs during the first catalytic subcycle of the natural substrate (ASD). To this end, the hydrogen abstraction-oxygen rebound

mechanism that takes place during hydroxylation of the ASD, has been also proposed as the mechanism for the hydroxylation of the EXE. With the results obtained, we have attempted to address different questions:

(i) Is the hydroxylation of EXE compatible with that observed for the ASD, in terms of activation energy?

According to the results derived from the analysis performed on the PES, the rate-limiting step during the hydroxylation reaction of EXE corresponds to the hydrogen abstraction process, as in the case of the hydroxylation of the ASD. In this step, the Cpd I oxidant species abstracts a hydrogen atom from the C_{19}-methyl group of the substrate, leading to the formation of an alkyl radical on the C_{19} carbon as well as of the iron-hydroxo complex. The activation barriers for this step, obtained through FEP techniques, show that it takes place through an endergonic process with activation barriers in the range of 16.9 kcal/mol (doublet) - 19.2 kcal/mol (quartet). When comparing these results to those obtained for the natural substrate, it is found that the activation barriers obtained for the ASD (13.5 kcal/mol for both doublet and the quartet) are around 3-5 kcal/mol lower than for the EXE. According to these findings, the hydroxylation reaction for the inhibitor proceeds through a slower process than for the natural substrate. These results are consistent with the experimental studies, from which it may be estimated an activation barrier for hydroxylation of the EXE 2.4 kcal/mol higher than for the hydroxylation of the ASD. Therefore, we can conclude that although this process is slower for the inhibitor than for the natural substrate, the hydroxylation of the EXE proceeds via the hydrogen abstraction-oxygen rebound mechanism as in the case of ASD.

(ii) Does the suicidal inhibition take place in this mechanistic step?

Since the hydroxylation of the EXE substrate is compatible with the mechanism proposed above, and the activation barriers are in the range of values expected, everything suggests that this is not the stage where the inhibition of the aromatase takes place. It has been reported that the EXE is a mechanism-based inactivator or suicidal inhibitor, thus it should irreversibly bind the active site of the enzyme at some stage. However, this behavior could not be observed throughout the hydroxylation process. Therefore, we dismiss the first catalytic subcycle of aromatase as the stage of the inhibition, and thus, it probably will take place in subsequent catalytic subcycles.

Furthermore, the fact that the products from the EXE hydroxylation show lower free energies than those obtained for the ASD suggests a competitive inhibition in the first subcycle of human aromatase.

(iii) How does the hydrophobic cleft affect to the activation energy of the process?

The examination of the different terms in which the activation energy can be decomposed, suggests that the electrostatic term is the only one involved in the stabilization of the transition state when compared with the reactant species. This finding obtained for the EXE substrate is not in accordance with that obtained for ASD, where the opposite behavior was observed. In the case of the latter, both the Lennard-Jones term and the polarization of the wave function are the responsible for such stabilization. Therefore, the role of the catalytic activity of aromatase during the hydroxylation of the EXE substrate lies in the stabilization of the TS by means of the electric field produced by the enzyme; while the role of this enzyme in the hydroxylation of the ASD consists of a stabilization of the TS by means of both polarization and dispersive effects.

Further analysis has revealed that the difference of the source of the catalytic activity between both substrates lies in two reasons: i) the presence of a methylidene group substituted in the C_6 of the EXE substrate, which mostly interacts with the surrounding amino acids of hydrophobic nature, and partly with a labile polar bridge that provides a binding region of electrostatic character. ii) The different orientation of the Thr-310 residue in both substrates. In the case of the EXE, the $O\gamma 1$ of this residue forms a hydrogen bond with a C_{19}-methyl hydrogen, which could set the position of this group throughout the reaction, thereby facilitating the hydrogen abstraction by the Cpd I.

5. Acknowledgements

This work was supported by MINECO Project CTQ2012-36253-C03-01, by Generalitat Valenciana *Prometeo*/2009/053 and *PrometeoII*/2014/022, and by Universitat Jaume I Project P1.1B2011-23. We acknowledge the Servei d'Informàtica of the Universitat Jaume I and BSC-Marenostrum (Application Id: QCM-2013-2-0044) for providing us with computer capabilities. I.V. thanks Spanish Ministerio de Ciencia e Innovación for a doctoral grant (CTQ2009-14541-C02).

Supporting Information

Selection of the main geometrical parameters obtained from PES calculations throughout the hydroxylation reaction. The Atomic Spin Densities of different atoms or fragments included in the QM model. In addition, a further analysis of the two different conformers observed for the Thr-310 residue has been performed. This analysis comprises the representation of the potential energy obtained from classical MD for each conformer, the decomposition of the Gibbs free energy into its different contributions for each conformer, as well as the snapshots corresponding to the reactant and TS that were found for each rotamer.

References

1. Meunier, B.; de Visser, S. P.; Shaik, S. Mechanism of oxidation reactions catalyzed by cytochrome P450 enzymes. *Chem. Rev.* **2004,** *104* (9), 3947-3980.
2. Ortiz de Montellano, P. R., *Cytochrome P450 structure, mechanism, and biochemistry*. Third edition ed.; Kluwer Academic/Plenum Publishers: New York, NY, USA, 2005.

3. Hrycay, E. G.; Bandiera, S. M., *Monooxygenase, peroxidase and peroxygenase properties and mechanisms of cytochrome*. 1 ed.; Springer International Publishing: 2015.
4. de Montellano, P. R. O. Hydrocarbon hydroxylation by cytochrome P450 enzymes. *Chem. Rev.* **2010,** *110* (2), 932-948.
5. Hrycay, E. G.; Bandiera, S. M. The monooxygenase, peroxidase, and peroxygenase properties of cytochrome P450. *Arch. Biochem. Biophys.* **2012,** *522* (2), 71-89.
6. Sligar, S. G.; Makris, T. M.; Denisov, I. G. Thirty years of microbial P450 monooxygenase research: Peroxo-heme intermediates - The central bus station in heme oxygenase catalysis. *Biochem. Biophys. Res. Commun.* **2005,** *338* (1), 346-354.
7. Simpson, E. R.; Clyne, C.; Rubin, G.; Boon, W. C.; Robertson, K.; Britt, K.; Speed, C.; Jones, M. Aromatase - A brief overview. *Annu. Rev. Physiol.* **2002,** *64* (1), 93-127.
8. Simpson, E. R.; Davis, S. R. Minireview: Aromatase and the regulation of estrogen biosynthesis - Some new perspectives. *Endocrinology* **2001,** *142* (11), 4589-4594.
9. Hong, Y.; Cho, M.; Yuan, Y. C.; Chen, S. Molecular basis for the interaction of four different classes of substrates and inhibitors with human aromatase. *Biochem. Pharmacol.* **2008,** *75* (5), 1161-1169.
10. Ghosh, D.; Lo, J.; Morton, D.; Valette, D.; Xi, J.; Griswold, J.; Hubbell, S.; Egbuta, C.; Jiang, W.; An, J., et al. Novel aromatase inhibitors by structure-guided design. *J. Med. Chem.* **2012,** *55* (19), 8464-8476.
11. Ghosh, D.; Griswold, J.; Erman, M.; Pangborn, W. Structural basis for androgen specificity and oestrogen synthesis in human aromatase. *Nature* **2009,** *457* (7226), 219-223.
12. Akhtar, M.; Skinner, S. J. The intermediary role of a 19-oxoandrogen in the biosynthesis of oestrogen. *Biochem. J* **1968,** *109* (2), 318-321.
13. Skinner, S. J.; Akhtar, M. The stereospecific removal of a C-19 hydrogen atom in oestrogen biosynthesis. *Biochem. J.* **1969,** *114* (1), 75-81.
14. Arigoni, D.; Battaglia, R.; Akhtar, M.; Smith, T. Stereospecificity of oxidation at C-19 in oestrogen biosynthesis. *J. Chem. Soc., Chem. Commun.* **1975,** *0* (6), 185-186.
15. Akhtar, M.; Calder, M. R.; Corina, D. L.; Wright, J. N. Mechanistic studies on C-19 demethylation in estrogen biosynthesis. *Biochem. J* **1982,** *201* (3), 569-580.
16. Akhtar, M.; Wright, J. N.; Lee-Robichaud, P. A review of mechanistic studies on aromatase (CYP19) and 17 alpha-hydroxylase-17,20-lyase (CYP17). *J. Steroid Biochem. Mol. Biol.* **2011,** *125* (1-2), 2-12.
17. Lu, A. Y. H.; Junk, K. W.; Coon, M. J. Resolution of the cytochrome P-450-containing ω-hydroxylation system of liver microsomes into three components. *J. Biol. Chem.* **1969,** *244* (13), 3714-3721.
18. Iyanagi, T. Structure and function of NADPH-cytochrome P450 reductase and nitric oxide synthase reductase domain. *Biochem. Biophys. Res. Commun.* **2005,** *338* (1), 520-528.
19. Hong, Y. Y.; Li, H. Z.; Yuan, Y. C.; Chen, S. A. Sequence-function correlation of aromatase and its interaction with reductase. *J. Steroid Biochem. Mol. Biol.* **2010,** *118* (4-5), 203-206.
20. Pandey, A. V.; Kempna, P.; Hofer, G.; Mullis, P. E.; Fluck, C. E. Modulation of human CYP19A1 activity by mutant NADPH P450 oxidoreductase. *Mol. Endocrinol.* **2007,** *21* (10), 2579-2595.
21. Surawatanawong, P.; Tye, J. W.; Hall, M. B. Density functional theory applied to a difference in pathways taken by the enzymes cytochrome P450 and superoxide reductase: Spin states of ferric hydroperoxo intermediates and hydrogen bonds from water. *Inorg. Chem.* **2010,** *49* (1), 188-198.
22. Vatsis, K. P.; Coon, M. J. Oxidative aldehyde deformylation catalyzed by NADPH-cytochrome P450 reductase and the flavoprotein domain of neuronal nitric oxide synthase. *Biochem. Biophys. Res. Commun.* **2005,** *337* (4), 1107-1111.
23. Akhtar, M.; Njar, V. C. O.; Neville Wright, J. Mechanistic studies on aromatase and related C-C bond cleaving P-450 enzymes. *J. Steroid Biochem. Mol. Biol.* **1993,** *44* (4–6), 375-387.
24. Akhtar, M.; Corina, D.; Miller, S.; Shyadehi, A. Z.; Wright, J. N. Mechanism of the acyl-carbon cleavage and related reactions catalyzed by multifunctional P-450s - studies on cytochrome-P-450(17-alpha). *Biochemistry* **1994,** *33* (14), 4410-4418.
25. Grinkova, Y. V.; Denisov, I. G.; Waterman, M. R.; Arase, M.; Kagawa, N.; Sligar, S. G. The ferrous-oxy complex of human aromatase. *Biochem. Biophys. Res. Commun.* **2008,** *372* (2), 379-382.
26. Gantt, S. L.; Denisov, I. G.; Grinkova, Y. V.; Sligar, S. G. The critical iron-oxygen intermediate in human aromatase. *Biochem. Biophys. Res. Commun.* **2009,** *387* (1), 169-173.

27. Sohl, C. D.; Guengerich, F. P. Kinetic analysis of the three-step steroid aromatase reaction of human cytochrome P450 19A1. *J. Biol. Chem.* **2010,** *285* (23), 17734-17743.
28. Guengerich, F. P.; Sohl, C. D.; Chowdhury, G. Multi-step oxidations catalyzed by cytochrome P450 enzymes: Processive vs. distributive kinetics and the issue of carbonyl oxidation in chemical mechanisms. *Arch. Biochem. Biophys.* **2011,** *507* (1), 126-134.
29. Khatri, Y.; Luthra, A.; Duggal, R.; Sligar, S. G. Kinetic solvent isotope effect in steady-state turnover by CYP19A1 suggests involvement of Compound I for both hydroxylation and aromatization steps. *FEBS Lett.* **2014,** *588* (17), 3117-3122.
30. Mak, P. J.; Luthra, A.; Sligar, S. G.; Kincaid, J. R. Resonance raman spectroscopy of the oxygenated intermediates of human CYP19A1 implicates a compound I intermediate in the final lyase step. *J. Am. Chem. Soc.* **2014,** *136* (13), 4825-4828.
31. Yoshimoto, F. K.; Guengerich, F. P. Mechanism of the third oxidative step in the conversion of androgens to estrogens by cytochrome P450 19A1 steroid aromatase. *J. Am. Chem. Soc.* **2014,** *136* (42), 15016-15025.
32. Hackett, J. C.; Brueggemeier, R. W.; Hadad, C. M. The final catalytic step of cytochrome P450 aromatase: A density functional theory study. *J. Am. Chem. Soc.* **2005,** *127* (14), 5224-5237.
33. Sen, K.; Hackett, J. C. Peroxo-iron mediated deformylation in sterol 14 alpha-demethylase catalysis. *J. Am. Chem. Soc.* **2010,** *132* (30), 10293-10305.
34. Lonsdale, R.; Oláh, J.; Mulholland, A. J.; Harvey, J. N. Does compound I vary significantly between isoforms of cytochrome P450? *J. Am. Chem. Soc.* **2011,** *133* (39), 15464-15474.
35. Elenewski, J. E.; Hackett, J. C. Cytochrome P450 compound I in the plane-wave pseudopotential framework: GGA electronic and geometric structure of thiolate-ligated iron(IV)–oxo porphyrin. *J. Comput. Chem.* **2013**, 1647-1660.
36. Krámos, B.; Oláh, J. Enolization as an alternative proton delivery pathway in human aromatase (P450 19A1). *J. Phys. Chem. B* **2013,** *118* (2), 390-405.
37. Krámos, B.; Oláh, J. The mechanism of human aromatase (CYP 19A1) revisited: DFT and QM/MM calculations support a compound I-mediated pathway for the aromatization process. *Struct. Chem.* **2015,** *26* (1), 279-300.
38. Sgrignani, J.; Iannuzzi, M.; Magistrato, A. Role of water in the puzzling mechanism of the final aromatization step promoted by the human aromatase enzyme. Insights from QM/MM MD simulations. *J. Chem. Inf. Model.* **2015,** *55* (10), 2218-2226.
39. Xu, K.; Wang, Y.; Hirao, H. Estrogen formation via H-abstraction from the O–H bond of gem-diol by compound I in the reaction of CYP19A1: Mechanistic scenario derived from multiscale QM/MM calculations. *ACS Catal.* **2015,** *5* (7), 4175-4179.
40. Viciano, I.; Castillo, R.; Martí, S. QM/MM modeling of the hydroxylation of the androstenedione substrate catalyzed by cytochrome P450 aromatase (CYP19A1). *J. Comput. Chem.* **2015,** *36* (23), 1736-1747.
41. Lombardi, P. Exemestane, a new steroidal aromatase inhibitor of clinical relevance. *Biochim. Biophys. Acta, Mol. Basis Dis.* **2002,** *1587* (2-3), 326-337.
42. Ciocca, D. R.; Fanelli, M. A. Estrogen receptors and cell proliferation in breast cancer. *Trends Endocrinol. Metab.* **1997,** *8* (8), 313-321.
43. Galeazzi, R.; Massaccesi, L. Insight into the binding interactions of CYP450 aromatase inhibitors with their target enzyme: A combined molecular docking and molecular dynamics study. *J. Mol. Model.* **2011**, 1-14.
44. Brueggemeier, R. W.; Hackett, J. C.; Diaz-Cruz, E. S. Aromatase inhibitors in the treatment of breast cancer. *Endocr. Rev.* **2005,** *26* (3), 331-345.
45. Brueggemeier, R. W.; Richards, J. A.; Joomprabutra, S.; Bhat, A. S.; Whetstone, J. L. Molecular pharmacology of aromatase and its regulation by endogenous and exogenous agents. *J. Steroid Biochem. Mol. Biol.* **2001,** *79* (1–5), 75-84.
46. Robinson, A. A review of the use of exemestane in early breast cancer. *Ther. Clin. Risk Manag.* **2009,** *5*, 91-98.
47. Chen, S. Aromatase and breast cancer. *Front. Biosci.* **1998,** *3*, d922-d933.
48. Santen, R. J.; Brodie, H.; Simpson, E. R.; Siiteri, P. K.; Brodie, A. History of aromatase: Saga of an important biological mediator and therapeutic target. *Endocr. Rev.* **2009,** *30* (4), 343-375.

49. Ahmad, I.; Shagufta Recent developments in steroidal and nonsteroidal aromatase inhibitors for the chemoprevention of estrogen-dependent breast cancer. *Eur. J. Med. Chem.* **2015,** *102*, 375-386.
50. Dowsett, M. Drug and hormone interactions of aromatase inhibitors. *Endocr. Relat. Cancer* **1999,** *6* (2), 181-5.
51. Hong, Y. Y.; Rashid, R.; Chen, S. A. Binding features of steroidal and nonsteroidal inhibitors. *Steroids* **2011,** *76* (8), 802-806.
52. Cepa, M.; da Silva, E. J. T.; Correia-da-Silva, G.; Roleira, F. M. F.; Teixeira, N. A. A. Synthesis and biochemical studies of 17-substituted androst-3-enes and 3,4-epoxyandrostanes as aromatase inhibitors. *Steroids* **2008,** *73* (14), 1409-1415.
53. Caporuscio, F.; Rastelli, G.; Imbriano, C.; Del Rio, A. Structure-based design of potent aromatase inhibitors by high-throughput docking. *J. Med. Chem.* **2011,** *54* (12), 4006-4017.
54. Ghosh, D.; Lo, J.; Egbuta, C. Recent progress in the discovery of next generation inhibitors of aromatase from the structure–function perspective. *J. Med. Chem.* **2015**.
55. Neves, M. A. C.; Dinis, T. C. P.; Colombo, G.; Melo, M. Fast three dimensional pharmacophore virtual screening of new potent non-steroid aromatase inhibitors. *J. Med. Chem.* **2009,** *52* (1), 143-150.
56. Roy, P. P.; Roy, K. Docking and 3D-QSAR studies of diverse classes of human aromatase (CYP19) inhibitors. *J. Mol. Model.* **2010,** *16* (10), 1597-1616.
57. Sgrignani, J.; Bon, M.; Colombo, G.; Magistrato, A. Computational approaches elucidate the allosteric mechanism of human aromatase inhibition: A novel possible route to small-molecule regulation of CYP450s activities? *J. Chem. Inf. Model.* **2014,** *54* (10), 2856-2868.
58. Brueggemeier, R. W. Overview of the pharmacology of the aromatase inactivator exemestane. *Breast Cancer Res. Treat.* **2002,** *74* (2), 177-185.
59. Field, M. J.; Albe, M.; Bret, C.; Proust-De Martin, F.; Thomas, A. The dynamo library for molecular simulations using hybrid quantum mechanical and molecular mechanical potentials. *J. Comput. Chem.* **2000,** *21* (12), 1088-1100.
60. Li, H.; Robertson, A. D.; Jensen, J. H. Very fast empirical prediction and rationalization of protein pKa values. *Proteins: Struct., Funct., Bioinf.* **2005,** *61* (4), 704-721.
61. Byrd, R. H.; Lu, P.; Nocedal, J.; Zhu, C. A limited memory algorithm for bound constrained optimization. *SIAM J. Sci. Comput.* **1995,** *16* (5), 1190-1208.
62. Dewar, M. J. S.; Zoebisch, E. G.; Healy, E. F.; Stewart, J. J. P. Development and use of quantum mechanical molecular models. 76. AM1: A new general purpose quantum mechanical molecular model. *J. Am. Chem. Soc.* **1985,** *107* (13), 3902-3909.
63. Jorgensen, W. L.; Maxwell, D. S.; Tirado-Rives, J. Development and testing of the OPLS all-atom force field on conformational energetics and properties of organic liquids. *J. Am. Chem. Soc.* **1996,** *118* (45), 11225-11236.
64. Jorgensen, W. L.; Chandrasekhar, J.; Madura, J. D.; Impey, R. W.; Klein, M. L. Comparison of simple potential functions for simulating liquid water. *J. Chem. Phys.* **1983,** *79* (2), 926-935.
65. Marti, S.; Moliner, V.; Tunon, I. Improving the QM/MM description of chemical processes: A dual level strategy to explore the potential energy surface in very large systems. *J. Chem. Theory Comput.* **2005,** *1* (5), 1008-1016.
66. Baker, J. Constrained optimization in delocalized internal coordinates. *J. Comput. Chem.* **1997,** *18* (8), 1079-1095.
67. Baker, J.; Kessi, A.; Delley, B. The generation and use of delocalized internal coordinates in geometry optimization. *J. Chem. Phys.* **1996,** *105* (1), 192-212.
68. Zhang, Y. K.; Liu, H. Y.; Yang, W. T. Free energy calculation on enzyme reactions with an efficient iterative procedure to determine minimum energy paths on a combined ab initio QM/MM potential energy surface. *J. Chem. Phys.* **2000,** *112* (8), 3483-3492.
69. Hay, P. J.; Wadt, W. R. Abinitio effective core potentials for molecular calculations - potentials for K to Au including the outermost core orbitals. *J. Chem. Phys.* **1985,** *82* (1), 299-310.
70. Becke, A. D. Density-functional thermochemistry .3. The role of exact exchange. *J. Chem. Phys.* **1993,** *98* (7), 5648-5652.
71. Miehlich, B.; Savin, A.; Stoll, H.; Preuss, H. Results obtained with the correlation energy density functionals of Becke and Lee, Yang and Parr. *Chem. Phys. Lett.* **1989,** *157* (3), 200-206.

72. Altun, A.; Kumar, D.; Neese, F.; Thiel, W. Multireference ab initio quantum mechanics/molecular mechanics study on intermediates in the catalytic cycle of cytochrome P450(cam). *J. Phys. Chem. A* **2008,** *112* (50), 12904-12910.
73. Chen, H.; Song, J. S.; Lai, W. Z.; Wu, W.; Shaik, S. Multiple low-lying states for compound I of P450(cam) and chloroperoxidase revealed from multireference ab initio QM/MM calculations. *J. Chem. Theory Comput.* **2010,** *6* (3), 940-953.
74. Shaik, S.; Kumar, D.; de Visser, S. P.; Altun, A.; Thiel, W. Theoretical perspective on the structure and mechanism of cytochrome P450 enzymes. *Chem. Rev.* **2005,** *105* (6), 2279-2328.
75. Shaik, S.; Cohen, S.; Wang, Y.; Chen, H.; Kumar, D.; Thiel, W. P450 enzymes: Their structure, reactivity, and selectivity-modeled by QM/MM calculations. *Chem. Rev.* **2010,** *110* (2), 949-1017.
76. M. J. Frisch; G. W. Trucks; H. B. Schlegel; G. E. Scuseria; M. A. Rob; J. R. Cheeseman; J. A. Montgomery Jr.; T. Vreven; K. N. Kudin; J. C. Burant, et al. *Gaussian 03*, Revision D.02; Gaussian, Inc.: Wallingford, CT, 2004.
77. Giudici, D.; Ornati, G.; Briatico, G.; Buzzetti, F.; Lombardi, P.; di Salle, E. 6-Methylenandrosta-1,4-diene-3,17-dione (FCE 24304): A new irreversible aromatase inhibitor. *J. Steroid Biochem.* **1988,** *30*, 391-394.
78. Filatov, M.; Harris, N.; Shaik, S. On the "rebound" mechanism of alkane hydroxylation by cytochrome P450: Electronic structure of the intermediate and the electron transfer character in the rebound step. *Angew. Chem. Int. Ed.* **1999,** *38* (23), 3510-3512.
79. Fishelovitch, D.; Hazan, C.; Hirao, H.; Wolfson, H. J.; Nussinov, R.; Shaik, S. QM/MM study of the active species of the human cytochrome P450 3A4, and the influence thereof of the multiple substrate binding. *J. Phys. Chem. B* **2007,** *111* (49), 13822-13832.
80. Phillips, J. C.; Braun, R.; Wang, W.; Gumbart, J.; Tajkhorshid, E.; Villa, E.; Chipot, C.; Skeel, R. D.; Kalé, L.; Schulten, K. Scalable molecular dynamics with NAMD. *J. Comput. Chem.* **2005,** *26* (16), 1781-1802.

Table of Contents Graphic

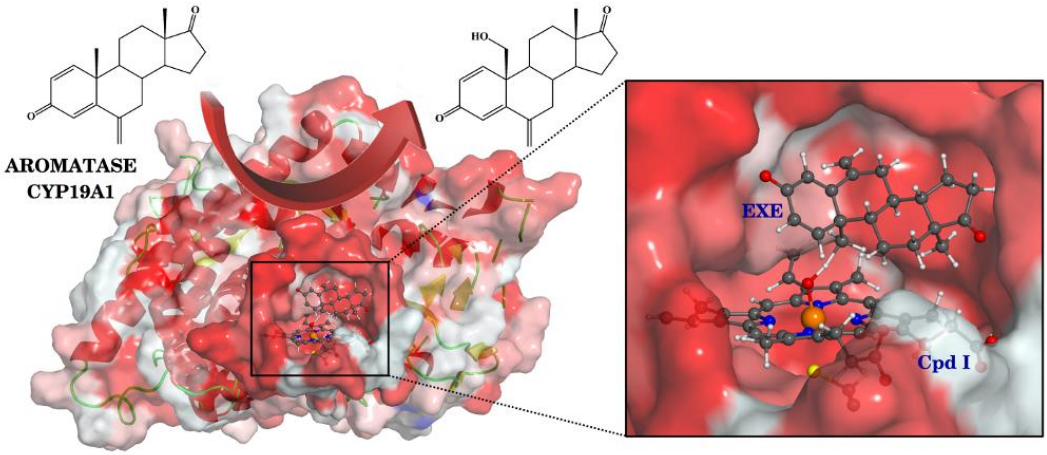
AROMATASE
CYP19A1
EXE
Cpd I